Simulation of Injection Mold Filling of Viscoelastic Polymer with Fountain Flow

Viscoelasticity, nonisothermality, and fountain flow influence the microstructure development during injection mold filling of polymer melts and, therefore, the ultimate properties of a molded article. A comprehensive two-dimensional mathematical model is developed to evaluate the effects of these factors on the structure of the flow field. Special consideration is given to the shape of the flow front, which is crucial in determining the structure of flow in the fountain region. The effects of slip and crystallization are also considered and their influence on model predictions are analyzed. Simulations using the no-slip and slip boundary conditions show that a slip boundary condition is necessary to alleviate the singularities in the flow structure. The results also indicate that the predicted stress profiles are significantly influenced by the viscoelasticity of the polymer melt. Furthermore, the nonisothermality and subsequent deposition of a solid layer next to the mold walls considerably alter the moldability parameters and the flow field.

M. R. Kamal, S. K. Goyal, E. Chu
Department of Chemical Engineering
McGill University
Montreal, Quebec H3A 2A7, Canada

Introduction

The microstructure of injection-molded articles is generally anisotropic and largely depends on crystallinity, orientation, and stress distributions induced during the molding cycle. The distribution of the microstructure is closely related to the thermal and deformation history of each fluid particle in the finished product. Although many attempts have been made in the last two decades to quantitatively describe the process of injection mold filling, most mathematical models do not usually incorporate some of the complex characteristics of real injection molding materials and processes (such as viscoelasticity, crystallinity, and nonisothermality) or the details of fountain flow and the shape of the melt front. The role of fountain flow during mold filling has been widely recognized to influence the microstructure of the molded article (Tadmor, 1974; and Schmidt, 1974).

The objectives of this work are twofold:

1. To present a comprehensive mathematical model for the transient mold filling process by incorporating viscoelasticity, crystallinity, nonisothermality, fountain flow, slip, and shape of the melt front.

2. To isolate and analyze the effects of the above factors on the structure of the flow field.

Correspondence concerning this paper should be addressed to M. R. Kamal.

Previous literature

Early work related to the present study can be grouped into three major categories:

1. Studies related to moldability criteria such as pressure drops, fill time, and position of the melt front

2. Studies related to nonisothermal effects using simplified rheological models

3. Studies related to the kinematics of fountain flow from purely the fluid dynamic point of view.

A large number of articles have covered these topics recently (Kamal and Lafleur, 1986; Kamal et al., 1986; Mavridis et al., 1986a; Coyle et al., 1987). For the sake of brevity, we will mainly be concerned here with those modeling studies that have attempted to include the characteristics of fountain flow in relation to injection mold filling. Table 1 provides a summary of previous work on injection mold filling with fountain flow. An examination of Table 1 reveals that many of the previous workers have used either the Newtonian fluid model (Manzione, 1981; Castro and Macosko, 1982; Givler et al., 1983; Behrens, 1983; Coyle, 1986; Coyle et al., 1987) or the power law fluid model (Tadmor, 1974; Gogos et al., 1986; Mavridis et al., 1986 a,b) with no account of viscoelasticity. The effect of nonisothermality was considered by Manzione (1981) and Castro and Macosko (1982) along with the Newtonian fluid model. Kamal and coworkers (Kamal et al., 1986; Kamal and Lafleur, 1986;

Table 1. Previous Work on Injection Mold Filling with Fountain Flow

Reference	Constitutive Eq.	Energy Eq.	Consideration of Slip	Shape of Flow Front	Crystallization	Method of Solution
Kamal et al. (1986) Kamal and Lafleur (1986) Lafleur and Kamal (1986)	White-Metzner (viscoelastic)	Yes	No	Flat	Yes	Marker-and-cell (finite-difference)
Gogos et al. (1986) Huang (1978)	Power law	No	No	Transient development	No	Marker-and-cell (finite-difference)
Mavridis et al. (1986a, b, c)	Newtonian, power law, and Carreau model	No	No	Curved (nearly semicircular)	No	Finite elements
Coyle (1986) Coyle et al. (1987)	Newtonian	No	No	Curved (nearly semicircular)	No	Finite elements
Behrens (1983)	Newtonian	No	No	Transient development, final shape: curved (nearly semicircular)	No	Finite elements
Givler et al. (1983)	Newtonian	No	No	Curved (nearly semicircular)	No	Finite elements
Castro and Macosko (1982)	Newtonian	Yes	No slip except at contact point	Flat	No	Analytic and finite-difference
Manzione (1981)	Newtonian	Yes	No	Curved (nearly semicircular)	No	Marker-and-cell (finite-difference)
Tadmor (1974)	Power law	No	No	Curved (semicircular)	No	Analytic
Present work	White-Metzner, power law	Yes	Yes	Transient development and curved (nearly semicircular)	Yes	Marker-and-cell (finite-difference)

Lafleur and Kamal, 1986) have included the effect of viscoelasticity and nonisothermality in their model of mold filling for crystallizing polymer melts.

Although the apparent slip phenomenon and the evolution of free surface shape appear to be crucial in any realistic simulation of fountain flow, many previous workers have not incorporated these aspects into mathematical modeling of injection mold filling. From a purely fluid dynamic viewpoint, it has been recognized, for more than 15 years, that a dynamic three-phase contact line exists where the interface between liquid and a second immiscible fluid intersects the solid surface, and the movement of contact lines violates the adherence, or no-slip boundary condition, that is otherwise obeyed by flowing liquids. This rheological anomaly has been discussed by several investigators (Huh and Scriven, 1971; Hoffman, 1975; Dussan V., 1976; Hocking, 1977; Huh and Mason, 1977; Metzner et al., 1979; Lowndes, 1980; Silliman and Scriven, 1980; Bach and Hassager, 1985), and many variations of the slip boundary condition have been employed to alleviate the singularities resulting from the no-slip boundary condition. Furthermore, various qualitative theories and arguments have been invoked to explain the slip phenomenon. Usually, these arguments are based on the physical system, kinetic theory, and thermodynamic considerations (Garner and Nissan, 1946; Busse, 1967; Silliman and Scriven, 1980).

In an attempt to quantitatively describe the fountain effect at the rear of an index, Bhattacharji and Savic (1965) have analyzed flow of Newtonian incompressible fluids between parallel plates using the Lagrangian frame of reference. Approximate analytical solutions were obtained using the full slip condition at the interface-wall contact point and the no-slip condition far from the interface. A careful examination of the expression for axial velocity, obtained by extending the analysis of Bhattacharji and Savic (1965) given in the Appendix, indicates finite and nonzero velocities at the wall even though an explicit slip boundary condition along the wall was not used in the fountain flow region. Furthermore, the results indicate that behind the contact point a fully developed parabolic velocity profile exists upstream at a distance that is approximately equal to the gap between the parallel plates.

In the mathematical modeling of injection mold filling with fountain flow, analysis of the interface shape under dynamic conditions is also important. In fact, the dynamic systems of interest can be divided into two distinct categories (Elliott and Riddiford, 1964; Hoffman, 1975):

1. Systems in which the melt front interface is driven at a constant velocity with a fixed equilibrium shape

2. Systems in which the interface shape evolves, under nonequilibrium conditions, as the melt front moves into the cavity until an equilibrium shape is achieved

Formulation of the free-surface boundary conditions and the methods of solution are quite different for the two distinct problems. Behrens (1983) and Gogos et al. (1986) used appropriate boundary conditions for the evolution of interface shape. Many of the other previous workers have used boundary conditions relevant to the interface with constant shape and velocity, as noted in Table 1.

In this paper, we present a detailed two-dimensional mathematical model of injection mold filling in a rectangular cavity that takes into account the effect of the slip boundary condition. Special consideration is given to the shape of the flow front. In the nonisothermal case, the model considers the moving boundary due to solidification of the polymer melt next to the mold walls. The treatment of solidification incorporates a nonisothermal crystallization model. The effect of viscoelasticity on the model predictions is analyzed by comparing the results obtained

with a White-Metzner constitutive equation to those obtained using a generalized power law constitutive equation. Furthermore, the effect of nonisothermality on the flow fields and on the motion of tracer lines is analyzed in detail. In the analysis of the various cases, actual material properties are employed, on the basis of experimental measurements. The variability of material properties due to temperature and strain rate is taken into consideration.

Mathematical Model

During the filling stage, a hot non-Newtonian polymer melt is driven into a cold empty cavity. Therefore, a detailed mathematical model of injection mold filling must consider the phenomena of unsteady state free-surface flow, and transient cooling. In the case of thin cavities, variations in the width direction can be neglected, and therefore two-dimensional equations of change may be employed to mathematically describe the mold filling process. In dimensionless form, the equations of change in the Cartesian coordinate system are written as follows:

Continuity

$$\frac{\partial U}{\partial X} + \frac{\partial W}{\partial Z} = 0 \tag{1}$$

Momentum

$$\frac{\partial U}{\partial t} + U\frac{\partial U}{\partial X} + W\frac{\partial U}{\partial Z} = -\frac{\partial P}{\partial X} - \frac{1}{N_{Re}}\left(\frac{\partial \tau_{xx}}{\partial X} + \frac{\partial \tau_{xz}}{\partial Z}\right) \tag{2}$$

$$\frac{\partial W}{\partial t} + U\frac{\partial W}{\partial X} + W\frac{\partial W}{\partial Z} = -\frac{\partial P}{\partial Z} - \frac{1}{N_{Re}}\left(\frac{\partial \tau_{xz}}{\partial X} + \frac{\partial \tau_{zz}}{\partial Z}\right) \tag{3}$$

Energy

$$\frac{\partial \theta}{\partial t} + U\frac{\partial \theta}{\partial X} + W\frac{\partial \theta}{\partial Z} = \frac{1}{N_{Re}N_{Pr}}\left(\frac{\partial^2\theta}{\partial X^2} + \frac{\partial^2\theta}{\partial Z^2}\right) + \frac{(\partial k/\partial\theta)}{kN_{Re}N_{Pr}}\left[\left(\frac{\partial\theta}{\partial X}\right)^2 + \left(\frac{\partial\theta}{\partial Z}\right)^2\right] - \frac{N_{Br}}{N_{Re}N_{Pr}}\left[\tau_{xx}\frac{\partial U}{\partial X} + \tau_{zz}\frac{\partial W}{\partial Z} + \tau_{xz}\left(\frac{\partial U}{\partial Z} + \frac{\partial W}{\partial X}\right)\right] \tag{4}$$

where the dimensionless parameters are defined, in conjunction with power law parameters, the power law index n, and the consistency index K, as:

$$N_{Re} = \frac{\rho(T)U_c^{2-n}L_c^n}{K(T)}$$

$$N_{Pr} = \frac{K(T)C_p(T)L_c^{1-n}}{k(T)U_c^{1-n}}$$

$$N_{Br} = \frac{K(T)U_c^{n+1}}{(T_m - T_w)k(T)L_c^{n-1}}$$

It is important to note that in the process of nonisothermal injection molding, the material parameters such as thermal conductivity k, specific heat C_p, consistency index K, and density ρ, are all functions of temperature. Therefore, in Eqs. 2–4, the dimensionless parameters N_{Re}, N_{Pr}, and N_{Br} are variable and must be calculated at each point using the prevailing temperature field. However, it is justifiable during the filling stage to assume that the polymer melt is incompressible and that body forces are negligible.

In order to solve the momentum and energy equations, which contain the components of the stress tensor, it is necessary to express various stresses in terms of velocity gradients and the fluid properties using an appropriate rheological constitutive equation. In the present work, we use two different constitutive equations:

1. A viscoelastic equation based on the White-Metzner (1963) modification of the Maxwell model, utilizing the Oldroyd derivative in the contravariant form
2. The generalized power law model

In generalized form, the White-Metzner equation is written as:

$$\vec{\vec{\tau}} + \lambda(\Pi)\frac{\delta\vec{\vec{\tau}}}{\delta t} = \eta(\Pi)\vec{\vec{\Delta}} \tag{5}$$

where the relaxation time λ, and the viscosity η are functions of both the temperature field and the second invariant of the flow field and are usually related through a modulus, so that $\lambda = \eta/G$. In fact, when the relaxation time λ is zero, Eq. 5 reduces to the generalized power law form in which the relaxation time is absent. In the two-dimensional flow, the second invariant of the rate of deformation tensor Π, is expressed as:

$$\vec{\vec{\Delta}}:\vec{\vec{\Delta}} = 4\left(\frac{\partial U}{\partial X}\right)^2 + 2\left(\frac{\partial U}{\partial Z} + \frac{\partial W}{\partial X}\right)^2 + 4\left(\frac{\partial W}{\partial Z}\right)^2 \tag{6}$$

In the process of mold filling, the shear rates are relatively high. Therefore, the power law relationship

$$\eta = K(T)(\Pi/2)^{(n-1)/2} \tag{7}$$

may be used to predict the temperature-dependent shear viscosity η (Middleman, 1979; Deiber and Schowalter, 1981).

The transient temperature fields continuously alter the flow field because of the variations in the viscosity field and the movement of solidified layer. These, in turn, influence the fountain flow and thus the distribution of orientation.

The mathematical model employed in the present study attempts to predict the evolution of the degree of crystallinity and its distribution in the deposited solid layer at the mold walls. For this purpose, the model incorporates the nonisothermal crystallization kinetic equation proposed by Nakamura et al. (1972):

$$\chi(t) = \chi(\infty)\left(1 - \exp\left\{-\left(\int_0^t K_A[T(\tau)]\,d\tau\right)^{n^*}\right\}\right) \tag{8}$$

where

$\chi(t)$ = degree of crystallinity at time t
$K_A(T)$ = parameter related to rate constant
n^* = Avrami exponent

Solution of the equations of motion and energy requires appropriate specification of the initial and boundary conditions.

Since the field variables are symmetric about the centerline, the solution is sought between the centerline and the top of the mold. In the present analysis, it is assumed that, behind the gate, a fully developed power law flow profile exists at a distance equal to the thickness between the mold walls. Therefore, for a constant flow rate Q, the equation for the velocity distributions may be written as:

$$U|_{o,z,t} = \left(\frac{Q}{W_c H_c}\right)\left(\frac{s+2}{s+1}\right)\left[1 - \left(\frac{2Z}{H_c}\right)^{s+1}\right] \tag{9}$$

where W_c is the width of the cavity and $s = 1/n$. Furthermore, it is assumed that at the entrance of the mold cavity the temperature is uniform in the transverse direction, that is,

$$\theta|_{o,z,t} = \theta_m \tag{10}$$

At the centerline, the transverse velocity component and both the longitudinal velocity and the pressure gradients in the transverse direction are zero. Therefore,

$$W|_{x,o,t} = 0 \tag{11}$$

$$\left.\frac{\partial U}{\partial Z}\right|_{x,o,t} = 0 \tag{12}$$

and

$$\left.\frac{\partial P}{\partial Z}\right|_{x,o,t} = 0 \tag{13}$$

Since the temperature distribution is symmetric about the centerline, we have

$$\left.\frac{\partial \theta}{\partial Z}\right|_{x,o,t} = 0 \tag{14}$$

Assuming a constant temperature of the mold wall, a boundary condition for the heat transfer, at the top of the mold, may be written as:

$$k_m\left(\frac{\partial \theta}{\partial Z}\right)\Big|_{x,H_c/2,t} = L_c h(\theta_w - \theta_{x,H_c/2,t}) \tag{15}$$

where k_m is the thermal conductivity of the melt and h is the overall heat transfer coefficient.

In order to incorporate the fountain effect in the flow front, special consideration is given to the boundary conditions at the top of the mold. Previous analytical solutions and experimental investigations (Bhattacharji and Savic, 1965; Winter and Wei, 1982) have shown that the fountain effect is limited to a distance that is approximately equal to one thickness of the cavity behind the melt-wall contact line. Therefore, the boundary at the top of the mold may be divided into two regions as shown in Figure 1: a no-slip region, and an apparent slip region. In the no-slip region, both the normal and tangential components of velocity vanish at the top boundary. Therefore,

$$U\Big|_{x,H_{c/2,t}} = 0 \tag{16}$$

$$W\Big|_{x,H_{c/2,t}} = 0 \tag{17}$$

However, in the slip region, only the normal component of velocity vanishes, since there is no flow through the top boundary. For the tangential component of velocity, a dynamic condition that allows slip at the wall may be used:

$$\eta\frac{\partial U}{\partial Z} = -L_c\beta(x')U \tag{18}$$

where the parameter β is the slip, or momentum transfer, coefficient, which may represent the extent of adhesion of the melt to the solid wall. β equal to zero corresponds to unimpeded tangential slip, whereas the limit $\beta \to \infty$ corresponds to imposing the no-slip boundary condition. This implies that the value of β varies from ∞ to 0 in the fountain flow region.

Although the potential of the dynamic condition has been recognized for quite some time, certain difficulties have blocked its use in practical numerical simulations. The foremost difficulty concerns the identification of a suitable function that correctly describes the variation of the slip coefficient β over the entire range of fountain flow. Examination of the limiting values of β suggests the possibility of an exponential dependence. However, in view of the complex physics of the flow near contact lines, it is not clear how to obtain such a formulation for non-Newtonian and viscoelastic flows. Under these circumstances, it may be appropriate to obtain approximate solutions by using an analytic function for β, which is derived for the Newtonian fluids.

Extending the analysis of Bhattacharji and Savic (1965) for Newtonian fluid, a suitable exponential function for β can be obtained as shown in the Appendix, that is:

$$\beta(x') = \left(\frac{6\eta}{H_c}\right)[e^{(2x'/H_c)\sqrt{5}} - 1] \tag{19}$$

where x' is the positive distance from the contact point to a point on the mold wall behind the flow front. Equation 19 shows that at $x' = 0, \beta = 0$, and as $x' \to \infty, \beta \to \infty$, as suggested above. Since by substituting Eq. 19 into Eq. 18 the slip condition, Eq. 18, becomes independent of viscosity, it would appear reasonable to assume that the form of $\beta(x')$ in the case of viscoelastic non-Newtonian fluids would not be too different from Eq. 19.

Finally, an appropriate specification of the boundary conditions at the flow front is required to determine the shape of the interface. As mentioned earlier, the unsteady flow of a polymer melt with a free surface can be divided into two distinct categories, one in which the front interface is driven at a constant velocity with a fixed equilibrium shape and the other in which the initial interface shape evolves, under nonequilibrium conditions, as the melt front moves into the cavity. For both cases, the physical principle states that no momentum flux should cross

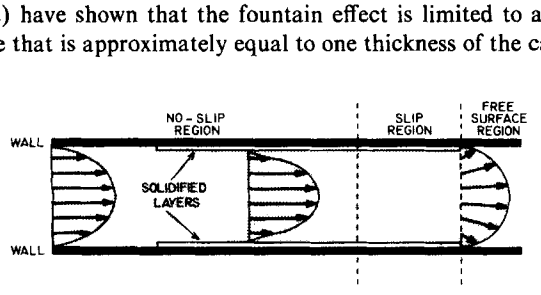

Figure 1. Various flow regimes.

the free surface of the melt. This implies that the normal and tangential stresses at the free surface must vanish. When the curvature of the free surface is small, the normal and tangenital stresses may be expressed in mathematical form as follows (Lafleur, 1983):

$$(P - P_e) - 2\eta\left(\frac{\partial V_n}{\partial n}\right) = 0 \tag{20}$$

$$\eta\left(\frac{\partial V_n}{\partial m} + \frac{\partial V_m}{\partial n}\right) = 0 \tag{21}$$

where n refers to the local outward normal direction of the free surface and m to the tangential direction. However, the corresponding procedures for solving the system of equations are quite different and are described as follows.

Case I

For the first case, the shape of the free surface is not known *a priori*, therefore Eqs. 20 and 21 may be used at any reasonably defined shape to obtain a solution. In order to obtain a solution for the unique shape, an additional condition is needed. In this case, an obvious additional condition which may be used is that the melt interface moves with a constant average velocity. In mathematical form, we may write

$$V_n = \text{constant (in Eulerian framework)}$$

or

$$V_n = 0 \text{ (in Lagrangian framework)} \tag{22}$$

While solving the equations of change to obtain the filed variables, a special strategy described in detail by Silliman and Scriven (1980) and Orr and Scriven (1978), is employed. First, a reasonably guessed shape of the free surface is chosen. The equations of change are solved using the assumed shape, but only two of the three boundary conditions, Eqs. 20 and 21, are used for convergence. The residual in the third boundary condition, Eq. 22, is then used to determine a new shape of the free surface. The calculations are repeated until all three boundary conditions are satisfied to a desired accuracy.

Case II

For the second case, in which the shape of the free surface evolves as the melt front moves into the cavity, the strategy of solution is different. In this case, the requirement that the melt front interface moves with a constant velocity is not needed. However, the initial shape of the interface is specified. A reasonable, and perhaps practical, choice of the initial shape of the interface is a flat profile. The equations of change in the Eulerian framework of coordinates are solved with the boundary conditions of Eqs. 20 and 21, and new velocities at the interface are calculated. Using the calculated velocities at the interface and the Lagrangian framework of coordinates, a new location of the interface is determined after time δt and the calculation process is repeated after each time interval.

In the following discussion, both of the above approaches were employed. Basically, they lead to similar results after a short duration of time.

Results and Discussion

Simulations were performed for injection mold filling of a commercial grade high-density polyethylene, Sclair 2908, supplied by DuPont of Canada Limited. A rectangular fan-gated mold cavity with dimensions 9.1 cm × 6.35 cm × 3.18 mm was used in the present calculations. Various physicochemical parameters used in the simulations were obtained through experiments. Table 2 gives the values of various parameters used in the present calculations.

The model equations described in the previous section were solved using the marker-and-cell method. The rectangular mold cavity (between the middle plane and the mold wall) was divided into 120 parts in the flow direction and 10 parts in the transverse direction for the finite-difference representation of the model equations. The present grid was found to be quite adequate for reasonably accurate determination of flow and temperature fields. For each time interval, the computing mesh extended from the gate up to the curved boundary at the melt interface. Figure 2 shows the computing mesh, where CP denotes the grid line (in the transverse direction) that passes through the melt-mold wall-air contact point at a particular instant of time. $CP + m$ denotes the grid line that is m grids ahead of the contact point, whereas $CP - n$ denotes the grid line that is n grids behind the contact point. For this moving mesh system, a computer code, McKAM-II, was developed and the computations were performed using a VAX 11/780 computer interfaced with an Applicon CAD/CAM/CAE system for continuous analysis and visual display of data in the melt front region.

Computations were performed to isolate and analyze the effects of various model parameters—slip, viscoelasticity, transient interface shape, nonisothermality, and crystallization—on the flow and temperature fields.

Effect of slip and viscoelasticity on flow field structure

In order to analyze the effects of slip and viscoelasticity on the flow field, without interference of thermal effects, the model equations were solved using isothermal mold filling conditions for the case in which the flow front interface moves with a constant velocity and an equilibrium shape.

Effect of Slip. The model equations were solved using the White-Metzner constitutive equation, and the no-slip and slip boundary conditions. Figure 3 compares the variation of longitudinal velocity in the flow direction using no-slip and slip boundary conditions. This figure shows a smooth deceleration of longitudinal velocity near the centerline using either of the two boundary conditions, but the profiles are quite different near the wall, as seen at grid lines 6 to 10 in the transverse direction. Using the slip boundary condition, the longitudinal velocity monotonically increases at locations that are near the mold wall in such a way that the velocity at the interface reaches a constant value and an equilibrium shape of the interface is maintained. However, the no-slip boundary condition produces an oscillatory behavior in longitudinal velocity at grid lines 6 to 9 and no change at grid line 10. Velocity profiles obtained by using the no-slip boundary condition may also result in unlimited elongation of the free surface, since the longitudinal velocities of fluid particles near the wall are much lower than the velocities near the centerline. These observations show that the slip boundary condition is necessary not only to alleviate the sin-

Table 2. Thermophysical Data, Transport Properties, Kinetic, and Other Parameters for Polyethylene (Sclair 2908) Used in Model

Property	Equation	Parameters
Viscosity, η, Pa · s	$\eta = A[\exp(\Delta E/RT)]\left(\frac{\Pi}{2}\right)^{n-1/2}$	$n = 0.822$ $A = 13.92$ kg · s^{n-2}/m $\Delta E/R = 2{,}167.4$ K
Thermal conductivity, k, W/m · K	$k = \sum_{i=0}^{m} A_i(T - 273.15)^i$ where T is in K	Solid phase: $m = 5$ $A_0 = 5.1528 \times 10^3$ $A_1 = -1.1389 \times 10^2$ $A_2 = 3.6453$ $A_3 = -5.7580 \times 10^{-2}$ $A_4 = 4.2367 \times 10^{-4}$ $A_5 = -1.1766 \times 10^{-6}$ Liquid phase: $m = 3$ $A_0 = -2.6526 \times 10^3$ $A_1 = 0.9418 \times 10^2$ $A_2 = -5.6777 \times 10^{-1}$ $A_3 = 1.1607 \times 10^{-3}$
Specific heat, C_p, J/kg · K	$C_p = B_0 + B_1 T$ where T is in K	$B_0 = 0.7314 \times 10^3$ $B_1 = 3.6314$
Heat transfer coefficient, h, W/m	—	$h = 9.32 \times 10^5$
Density, ρ, kg/m^3	$\rho = \sum_{i=0}^{2} A_i P^i$ where P is in Pa.	Temp. Range, °C: A_0, A_1, A_2 ≤140: 799.8, 1,023.3, −4,025.5 140–150: 793.1, 1,123.7, −5,432.1 150–160: 790.7, 966.0, −2,853.6 160–170: 785.2, 972.6, −2,797.7 170–180: 777.3, 1,123.5, −4,657.2 180–190: 772.9, 1,017.3, −2,954.4 190–200: 765.9, 1,051.8, −2,991.4
Crystallization kinetics	See Eq. 8 $K_A(T) = [Z(T)]^{1/n^*}$ $\text{Log}[Z(T)] = \sum_{i=0}^{3} A_i T^i$ where T is in K $\chi(\infty) = \sum_{i=0}^{2} B_i(T - 273.15)^i$ where T is in K	$n^* = 2$ $A_0 = -3508.02$ $A_1 = 13.47$ $A_2 = 7.32$ $A_3 = -1.31 \times 10^{-5}$ 353.15 K ≤ T ≤ 387.15 K $B_0 = 97.8060191$ $B_1 = -1.46177836$ $B_2 = 0.010067111$ 387.15 K ≤ T ≤ 394.15 K $B_0 = 2{,}223.2027$ $B_1 = -34.2745261$ $B_2 = 0.134416969$
Relaxation modulus, G, Pa	$\lambda = \eta/G$	$G = 10^5$
Flow rate, Q, m^3/s		$Q = 20.68 \times 10^{-6}$
Dimensionless time step, δt		δt = 1/4 (average time required by the fluid to pass a grid)

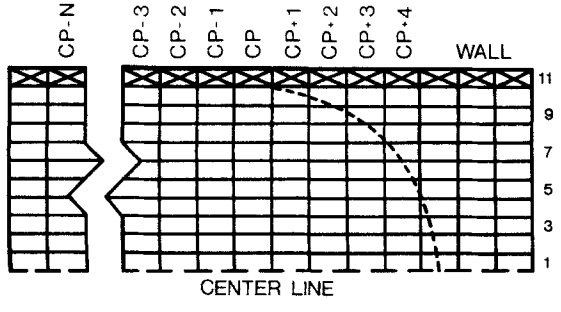

Figure 2. Finite-difference computing mesh pattern used in present simulation.

CP: grid line that passes through melt-mold wall-air contact point at a particular instant of time

gularity at the contact point, and thus the oscillatory behavior, but also to maintain an equilibrium shape of the melt front interface.

Transverse velocity profiles obtained using the no-slip and slip boundary conditions are compared in Figure 4. These results show that the maximum transverse velocity occurs at grid line *CP* between the centerline and the mold wall when the slip boundary condition is used, whereas much higher transverse velocities are predicted ahead of grid line *CP* when the no-slip boundary condition is used. Thus, by incorporating the slip boundary condition, the velocity rearrangement in the fountain flow region starts well behind the contact point *CP* and continues until the melt front interface is reached. On the other hand, the no-slip boundary condition produces velocity rearrangement largely in the region bounded by the grid line *CP* and

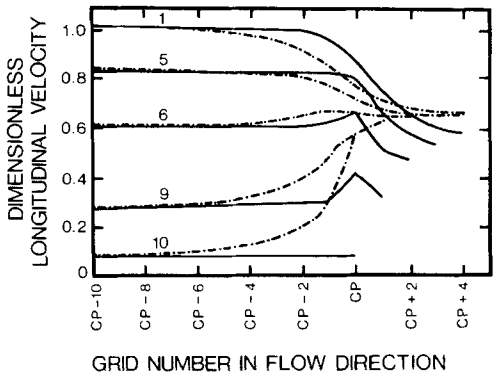

Figure 3. Variation of longitudinal velocity in flow direction.

No-slip and slip boundary conditions and White-Metzner constitutive equation under isothermal conditions
———— no-slip boundary condition
—·—·—·— slip boundary condition

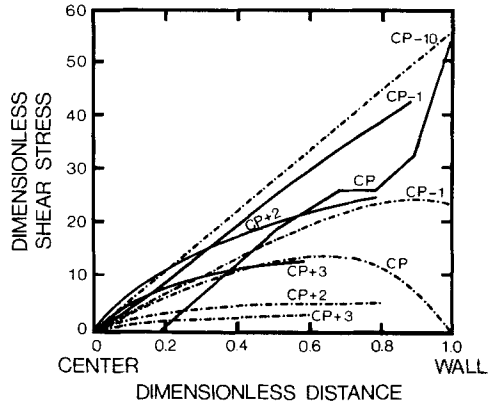

Figure 5. Shear stress profiles at various grid line positions.

No-slip and slip boundary conditions and White-Metzner constitutive equation under isothermal conditions
———— no-slip; —·—·—·— slip

the melt front interface. The results obtained by using the slip boundary condition are in qualitative agreement with the analytic solution obtained by Bhattacharji and Savic (1965) for reverse fountain flow.

Figure 5 shows a comparison of shear stress profiles obtained using no-slip and slip boundary conditions. This figure shows that at approximately one mold thickness behind the contact point, the shear stress varies linearly from the centerline to the wall because of the one-dimensional flow in the no-slip region. At the grid line, which passes through contact point *CP*, the no-slip condition predicts an oscillatory and discontinuous shear stress profile. However, the slip boundary condition provides smoothly curved shear stress profiles in the two-dimensional fountain flow region. Furthermore, it is interesting to note that in the grid line which passes through the contact point *CP*, the shear stress is zero at the centerline as well as at the wall and it is maximum at some point between the centerline and the mold wall. As expected, the shear stress diminishes as the free surface is approached.

Effect of Viscoelasticity. In order to quantitatively analyze the effect of viscoelasticity on flow fields and stress profiles, computations were performed using the generalized power law (inelastic) and the White-Metzner (viscoelastic) constitutive equations. The slip boundary condition was used in both cases. Simulations using either of the two constitutive equations produced essentially the same longitudinal velocity profiles. However, slight quantitative differences were noted in the transverse velocity profiles, as shown in Figure 6.

Figure 7 compares the shear stress profiles obtained using the generalized power law and the White-Metzner constitutive equations. As seen from Figure 7, both constitutive equations produced essentially the same shear stress profiles far behind the melt front region. This result is expected because essentially one-dimensional flow prevails in this region. However, the differences in shear stress profiles were quite large in the two-dimensional fountain flow region. Up to one mold thickness behind the grid line *CP*, the White-Metzner constitutive equation predicts much lower shear stresses near the mold wall than those predicted using the power law model.

The two different constitutive equations produced significantly different profiles for the differences in normal components of the stress tensor ($\tau_{zz} - \tau_{xx}$). The difference in profiles was noted both qualitatively and quantitatively. Near the wall, the magnitude of ($\tau_{zz} - \tau_{xx}$) increased at upstream positions

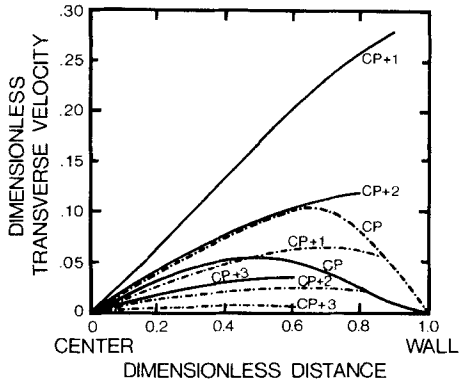

Figure 4. Transverse velocity profiles at various grid line positions.

No-slip and slip boundary conditions and White-Metzner constitutive equation under isothermal conditions
———— no-slip boundary condition
—·—·—·— slip boundary condition

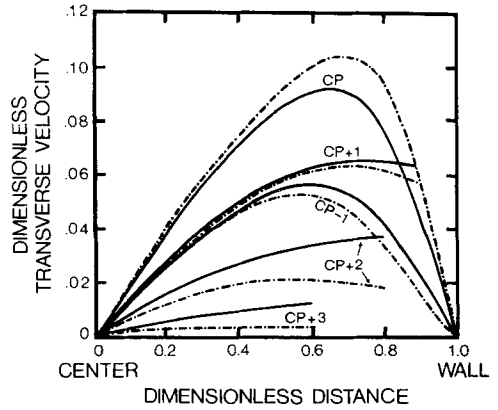

Figure 6. Transverse velocity profiles.

White-Metzner and generalized power law constitutive equations with slip boundary condition and isothermal conditions
———— power law; —·—·—·— White-Metzner

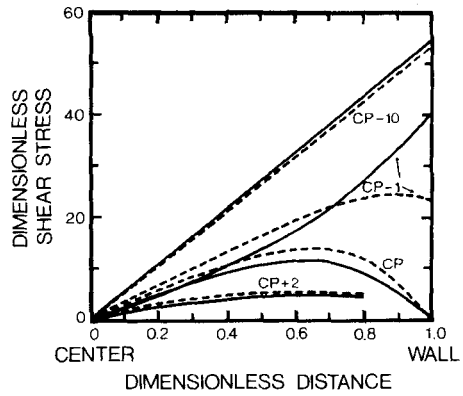

Figure 7. Shear stress profiles.
White-Metzner and generalized power law constitutive equations with slip boundary condition and isothermal conditions
———— power law; --- White-Metzner

behind the grid line *CP* using the White-Metzner equation, Figure 8, whereas it decreased, approaching zero, employing the generalized power law model. This supports the contention that the power law model does not predict normal stresses in simple shear or fully developed one-dimensional flows (Tadmor and Gogos, 1979). It is interesting to note that in both cases the magnitude of $(\tau_{zz} - \tau_{xx})$ tends to zero as the fluid particles approach the free surface. Furthermore, it is also noteworthy that the values of $(\tau_{zz} - \tau_{xx})$ are positive near the wall, whereas the values are negative near the centerline. This shows that the fluid particles will be extended in the flow direction near the wall, whereas the extension near the centerline will be in the transverse direction.

Evolution of melt front shape

The evolution of fluid interface for the transient fountain flow was simulated assuming a flat initial interfacial shape. As mentioned earlier, in this case the surface boundary condition, Eq. 22, was not used. Instead, using the marker-and-cell method the

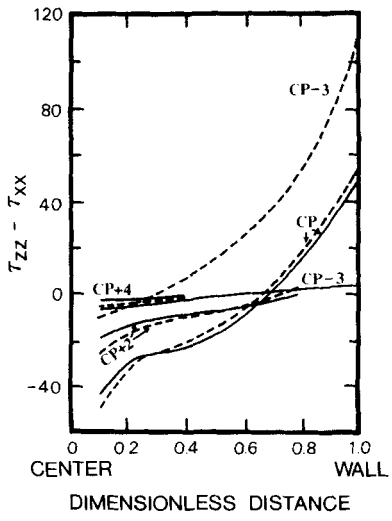

Figure 8. Profiles for difference in normal components of stress tensor $(\tau_{zz} - \tau_{xx})$.
White-Metzner and generalized power law constitutive equations with slip boundary condition and isothermal conditions
———— power law; --- White-Metzner

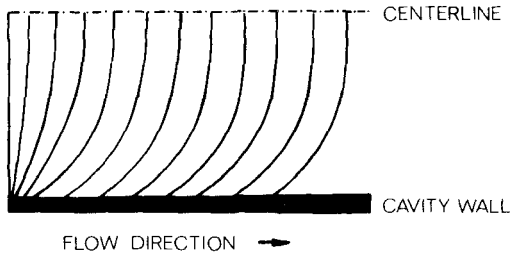

Figure 9. Evolution of shape of melt front interface with time.

movement of markers was governed by the calculated instantaneous velocity fields at the fluid interface. It is important to note that the transverse velocities at any point along the mold wall (including the contact point) are zero, and thus there is no possibility of any fluid spilling through the solid wall. Therefore, the contact point was moved along the mold wall by the instantaneous longitudinal velocity of the fluid particle at the contact point. Since the slip boundary condition was used in the calculations, the longitudinal velocity of the contact point did not remain zero after the flow was started and it increased with time as the interfacial shape evolved.

The instantaneous positions of the markers were frozen at different times using a graphics display screen (Applicon 4635). Figure 9 shows the evolution of the shape of the melt front interface with time during mold filling. It can be seen that the interfacial meniscus shape quickly changes from flat to a nearly semicircular shape as the polymer progresses inside the cavity.

Effect of nonisothermal conditions on flow field structure

As the hot polymer melt moves into the cold cavity, temperature profiles develop and the lowest temperatures are located at the mold wall. The developed temperature fields in turn influence the flow field due to changes in material properties. The flow field is also influenced by the formation of a solid layer near the mold walls because of cooling and crystallization.

Typical temperature profiles developed during transient nonisothermal melt flow are shown in Figure 10. This figure also illustrates the effect of fountain flow on the temperature fields in the flow front region. The present model predicts that at some

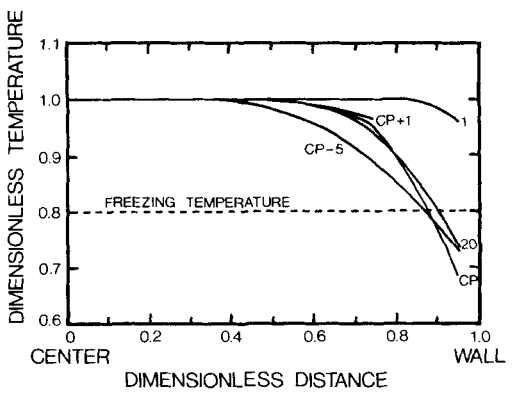

Figure 10. Temperature profiles at various grid line positions.
Slip bondary condition and White-Metzner constitutive equation

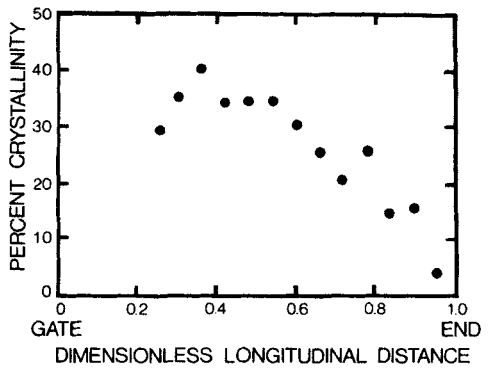

Figure 11. Crystallinity profile in skin layer during non-isothermal injection mold filling.

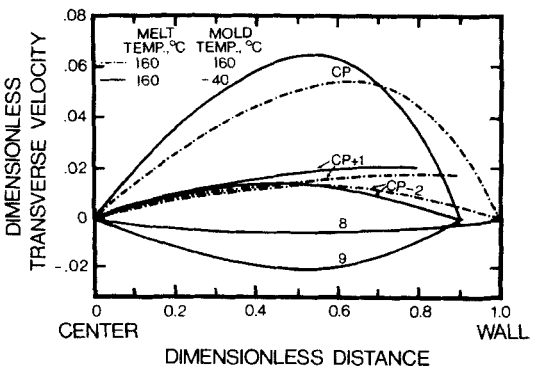

Figure 13. Effect of formation of solid layer on transverse velocity profiles.
White-Metzner constitutive equation and slip boundary condition

locations between the centerline and the mold wall, the temperatures in the fountain flow region are higher than those at the upstream positions. This may be explained by the fact that the fountain flow allows the hot melt to move from the center of the mold to the cavity walls and mix with the melt transported from the upstream.

Assuming an average solidification temperature of the high-density polyethylene of 120°C, it was predicted that a layer, 0.016 cm, of solid polymer would be deposited between the 21st and the 116th cells at the end of filling, for the molding conditions of 160/−40°C. Figure 11 gives the corresponding estimated crystallinity distribution in this layer. It shows that the degree of crystallinity increases near the gate, reaching a maximum value, and then decreases toward the end of the cavity. This may be explained by the fact that according to Eq. 8, the degree of crystallinity mainly depends on two variables; the time of cooling and the temperature of crystallization. During nonisothermal mold filling, the fluid particles that are farther from the gate will have more time for cooling, but lower temperatures. On the other hand, the fluid particles that are nearer the gate will have less time for cooling but higher temperatures. Therefore, the maximum crystallinity should occur somewhere between the gate and the end of the cavity. This is in agreement with experimental observations by Moy (1980).

The quantitative effects of temperature fields on the longitudinal and transverse velocity profiles are depicted in Figures 12 and 13, respectively. For a constant volumetric flow rate at the gate, the magnitudes of the longitudinal and transverse velocities are altered for the following two reasons. First, the viscosity of fluid particles near the mold wall increases due to lower temperatures in that region. Second, the total cross-sectional flow area is reduced due to the formation of the solid layer at the wall. Therefore, behind the fountain flow region the fluid particles tend to move toward the centerline, creating a slightly convergent channel flow. This in turn generates negative transverse velocities, Figure 13, and thus the magnitude of the longitudinal velocity in the core of the cavity increases, Figure 12. Furthermore, the velocity profiles shift toward the centerline due to the formation of the solid layer at the wall.

The effect of melt and mold temperatures on the predicted pressures at the gate is shown in Figure 14. This figure indicates that much higher gate pressures are required for nonisothermal molding conditions of 160/−40°C as compared to isothermal molding conditions of 160/160°C. The gate pressures required to fill the cavity decreased when the melt temperature was increased to 190°C.

In recent papers, Mavridis et al. (1986c) and Coyle et al. (1987) have simulated motion of tracer lines in two-dimensional fountain flow for isothermal Newtonian liquids using the finite-element method with no-slip boundary conditions. Using the present model, similar tracer simulations were performed for the crystallizing viscoelastic melt using the marker-and-cell finite-

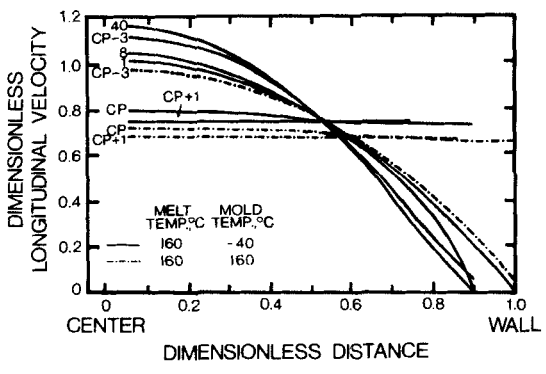

Figure 12. Effect of formation of solid layer on longitudinal velocity profiles.
White-Metzner constitutive equation and slip boundary condition

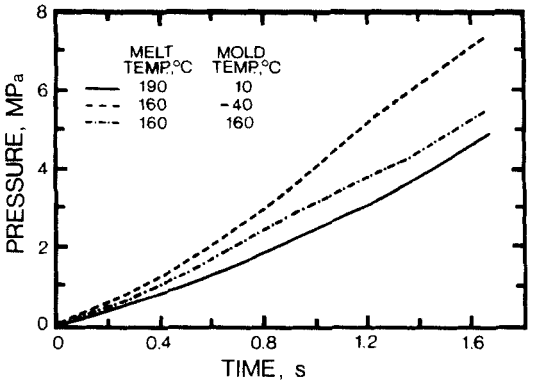

Figure 14. Effect of melt and mold temperatures on pressure profiles.
White-Metzner constitutive equation and slip boundary condition

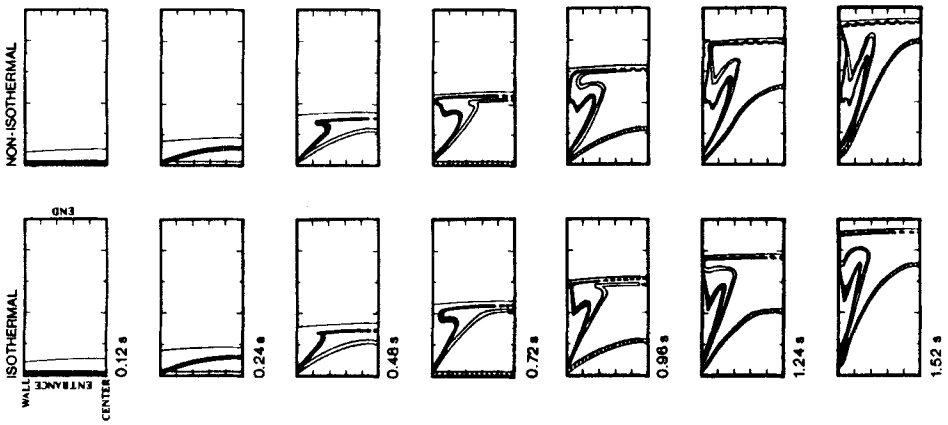

Figure 15. Sequence of tracer line deformations for isothermal and nonisothermal conditions at various times during filling.

White-Metzner constitutive equation and slip boundary condition

difference method with slip boundary conditions. The simulated tracer line movements for isothermal (160/160°C) and nonisothermal (160/−40°C) molding conditions are compared in Figure 15. This figure provides a sequence of instantaneous frames that illustrate the shapes and the locations of tracer lines at different times. Surprisingly, the extended mushroom shapes and the V-shaped protrusions near the cavity walls obtained in the present numerical experiments under isothermal conditions are similar to those obtained by Coyle et al. (1987), in spite of the fact that those authors used the Newtonian fluid and no-slip boundary conditions. The question of two entirely different constitutive equations producing similar tracer line deformations may be settled by reaffirming the arguments of Coyle et al. (1987) that viscoelasticity probably has little effect on the overall kinematics of fountain flow (other than changing the length scales) and the flow is largely determined by conservation of mass rather than by conservation of momentum. However, the question of two different boundary conditions—slip and no-slip—giving similar tracer line deformations seems more intriguing and requires a fundamental investigation into the ways in which the two different methods are used to obtain the solutions. The explanation of this may be found in the nature of the assumptions employed in the formulation of the finite-element and finite-difference methods. In particular, in the finite-element method, the effect of the slip and no-slip boundary conditions may be "seen" only in those elements that are in the immediate neighborhood of the wall. This fact is reflected in the results of Mavridis et al. (1986a), in the sense that although the stream function, velocity, and pressure profiles show smooth variations in the major part of the fountain flow region, the pressure profiles (which are largely dependent on the conservation of momentum) near the wall are highly unstable and oscillatory using the no-slip boundary condition. Thus, except in the immediate neighborhood of the wall, the finite-element method used with the no-slip boundary condition may provide flow field and tracer line deformations similar to those obtained by using the finite-difference method with the slip boundary condition.

In the case of nonisothermal conditions, the shapes of tracer line deformations are somewhat different. As shown in Figure 15, the first V-shaped protrusions that are formed near the mold wall become frozen in the solidified layer. Since the flow still persists beneath the solidified layer, a second V-shaped protrusion emerges. This behavior is quite different from that seen under isothermal conditions.

Effects of flow field on microstructure development

The marker-and-cell technique has an additional advantage in the sense that the fluid particles at any desired position can be tagged and their movement can be followed through time. This distinct feature of the technique can be used to understand the development of the microstructure during mold filling.

Figure 16 presents a manifestation of the fountain flow on the movement of fluid particles during mold filling. Numerical experiments were conducted to observe the movement of two sets of tracers injected at two different times. Figure 16 shows that the first set of tracers (solid symbols) are found located at the wall near the gate, while the second set of tracers (open symbols), injected at a later time, are found away from the gate. Thus, the order of the tracers at the wall is reversed. This phenomenon was first observed experimentally by Schmidt (1974) and can be simulated mathematically as shown here. Furthermore, it is interesting to note that the tracers remain distinct as they are deformed in the fountain flow region. In other words, there is no mixing of the tracers or buildup one beneath the other.

Another manifestation of the fountain flow is shown in Figure

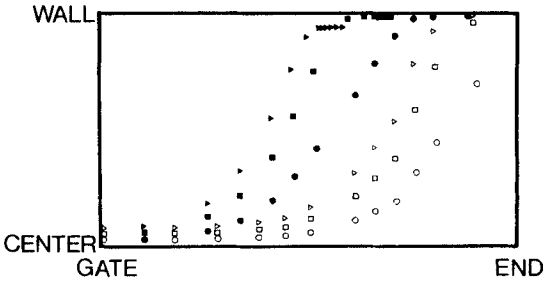

Figure 16. Effect of fountain flow on movement of tracers injected at two different times.

White-Metzner constitutive equation and slip boundary condition

● ■ ▲ injected at 0.12 s

○ □ △ injected at 0.24 s

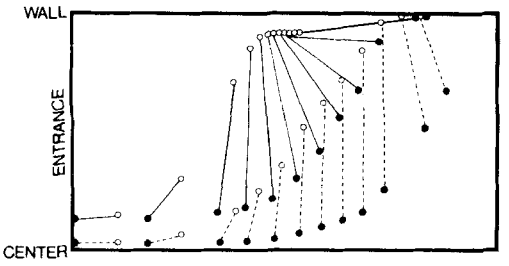

Figure 17. Effect of fountain flow on stretching and orientation of fluid particles.
White-Metzner constitutive equation and slip boundary condition

17 in terms of the effect of shear and elongational flow on the stretching and orientation of the fluid particles. Two pairs of markers were placed near the centerline a certain distance apart and oriented in the flow direction. For the sake of clarity, each pair is connected by a straight line. A careful examination of Figure 17 shows that as the markers encounter fountain flow, the distance between the markers (associated with the same pair) first increases, then decreases, and again increases as they reach near the wall. This phenomenon may be explained by considering the transverse and longitudinal velocity profiles in the fountain flow region. As shown in Figure 4, the maximum transverse velocity occurs somewhere between the centerline and the mold wall. The first stretching of the distance between the two markers is associated with the increase in the transverse velocity of fluid particles as they travel from the centerline toward the wall. After the maximum is reached, the transverse velocity decreases and so does the stretching between the markers. As a pair of markers reaches the wall, the effect of increase in the longitudinal velocity becomes predominant and the distance between the markers is further stretched, but at this time in the axial direction. Furthermore, it is interesting to note that a pair of markers changes its orientation as it moves in the fountain flow region, and near the wall the orientation is almost 180°. These observations may also be related to the experimental results of shrinkage in the molded articles obtained by Menges and Wübken (1973). These authors have found that the shrinkage of the polymer first increases as one approaches from the centerline toward the mold wall, then decreases, and again increases just near the mold wall.

Conclusions

A comprehensive mathematical model and a computer code, McKAM II, have been developed for an engineering analysis of injection mold filling of polymers. The model can predict the details of flow structure, pressure and temperature distributions, and crystallization during the filling stage. The results have indicated that in the fountain flow region, it is necessary to use a slip boundary condition to alleviate the singularities resulting from the no-slip boundary condition and to maintain the shape of the flow front. The shape of the melt front interface quickly becomes nearly semicircular as the polymer flows into the cavity. The results obtained using the White-Metzner constitutive equation and the generalized power law model have shown that the predicted stress profiles are significantly influenced by the constitutive equation used and by relaxation effects. Therefore, these effects must be considered when it is desired to predict the orientation of the molecules and/or the residual stresses that are directly influenced by the first normal stress difference and shear stress distributions during the filling stage.

During nonisothermal injection mold filling, the developed temperature profiles and subsequent deposition of the solid layer next to the mold walls considerably affect the moldability parameters and the flow field. Therefore, to obtain models of microstructure development during the injection molding process, the nonisothermal deformation history of polymer melts must be considered.

Acknowledgment

Financial support provided by the Ministère de l'Enseignement Supérieur de la Science et de la Technologie, Gouvernement du Québec, and the Natural Sciences and Engineering Research Council of Canada is greatly appreciated.

Notation

C_p = specific heat
G = relaxation modulus
h = overall heat transfer coefficient
H_c = thickness of cavity
k = thermal conductivity
K = consistency index
K_A = Nakamura's rate constant
L_c = length of cavity
n = power law index
n^* = Avrami exponent
N_{Br} = Brinkman number
N_{Pr} = Prandtl number
N_{Re} = Reynolds number
P = hydrostatic pressure
P_e = external pressure at free surface
Q = flow rate
s = constant = $1/n$
t = dimensionless time, $U_c t^*/L_c$
t^* = time
T_m, T_w = melt, wall temperatures
U = dimensionless longitudinal velocity, u_x/U_c
U_{avg} = dimensionless average velocity, u_{avg}/U_c
U_c = characteristic velocity
V_m, V_n = local velocity components tangential and normal to free surface
W = dimensionless transverse velocity, u_z/U_c
W_c = width of cavity
x' = rectangular coordinate toward fully developed flow, starting from contact point
X = rectangular coordinate in flow direction, x/L_c
Z = rectangular coordinate in transverse direction, z/L_c

Greek letters

β = slip coefficient
$\vec{\vec{\Delta}}$ = dimensionless rate of deformation tensor, $L_c\vec{\vec{\Delta}}^*/U_c$
$\vec{\vec{\Delta}}^*$ = rate of deformation tensor
η = viscosity
θ = dimensionless temperature, $(T - T_w)/(T_m - T_w)$
λ = relaxation time
Π = dimensionless second invariant of the rate of deformation tensor, $L_c^2(\Pi^*)/U_c^2$
Π^* = second invariant of the rate of deformation tensor
ρ = density
$\vec{\vec{\tau}}$ = dimensionless stress tensor
τ_{ij} = components of dimensionless stress tensor, $\tau_{ij}^* L_c^n/K_c U_c^n$
τ_{ij}^* = components of stress tensor
χ = degree of crystallinity
ψ = stream function

Appendix

Analytical solutions for viscous, incompressible two-dimensional fountain flow in rectangular channels of semiinfinite extent were obtained in terms of stream function by Bhattacharji and Savic (1965). After formulation with appropriate assumptions, solutions of the biharmonic equation

$$\nabla^4\psi = 0 \tag{A1}$$

were sought in the Lagrangian frame of reference subject to the following boundary conditions:

$$u_{x'} = \frac{\partial\psi}{\partial z} = u_{avg} \quad \text{for } z = H_c/2 \quad \text{and} \quad x' = \text{large} \tag{A2}$$

$$= 0 \quad \text{for } x' = 0 \tag{A3}$$

$$w_z = -\frac{\partial\psi}{\partial x'} = 0 \quad \text{for } z = H_c/2 \tag{A4}$$

$$\frac{\partial^2\psi}{\partial z^2} = 0 \quad \text{for } z = 0 \text{ (symmetry condition)} \tag{A5}$$

where x' and z are axial and transverse coordinates, respectively. A coordinate system was chosen such that $x' = 0$ at the contact point, and $z = 0$ at the centerline. Using the eigenfunctions of the biharmonic in Cartesian coordinates, the following solution was obtained for the stream function:

$$\psi = \frac{2u_{avg}}{\pi}\int_0^\infty \frac{(H_c/2)\cosh(H_c/2)p \cdot \sinh pz - z\sinh(H_c/2)p\cosh pz}{p[\cosh(H_c/2)p \cdot \sinh(H_c/2)p - (H_c/2)p]}\sin px'\,dp \tag{A6}$$

By developing the hyperbolic functions into a power series and then using the Fourier integral expression, an approximate expression for the stream function was obtained from Eq. A6.

$$\psi = \frac{u_{avg}z}{2}\left(1 - \frac{4z^2}{H_c^2}\right)[1 - e^{-(2x'/H_c)\sqrt{5}}] \tag{A7}$$

Differentiating Eq. A7 with respect to z, we get an expression for the axial velocity profile in the Lagrangian framework:

$$u_{x'} = \frac{\partial\psi}{\partial z} = \frac{u_{avg}}{2}\left(1 - \frac{12z^2}{H_c^2}\right)[1 - e^{-(2x'/H_c)\sqrt{5}}] \tag{A8}$$

When u_{avg} is added to Eq. A8, the frame of reference in which the walls of the channel are stationary is reestablished. Therefore, in the Eulerian framework:

$$u_{x'} = \frac{u_{avg}}{2}\left(1 - \frac{12z^2}{H_c^2}\right)[1 - e^{-(2x'/H_c)\sqrt{5}}] + u_{avg} \tag{A9}$$

It is interesting to note that although no explicit slip condition is used along the channel walls, Eq. A9 indicates finite and nonzero axial velocities at the wall in the fountain flow region.

An expression for the slip coefficient $\beta(x')$ in Eq. 18 can be obtained as follows. Differentiating Eq. A9 with respect to z, we get:

$$\frac{\partial u_{x'}}{\partial z} = -12u_{avg}\frac{z}{H_c^2}[1 - e^{-(2x'/H_c)\sqrt{5}}] \tag{A10}$$

Substituting Eq. A10 into Eq. 18, and evaluating the resulting expression at $z = H_c/2$, we get

$$\beta(x') = \left(\frac{6\eta}{H_c}\right)\left(\frac{u_{avg}}{u_{x'}}\right)_{z=H_c/2}[1 - e^{-(2x'/H_c)\sqrt{5}}] \tag{A11}$$

From Eq. A9

$$\left(\frac{u_{avg}}{u_{x'}}\right)_{z=H_c/2} = e^{(2x'/H_c)\sqrt{5}} \tag{A12}$$

Substituting Eq. A12 into Eq. A11, we obtain an expression for the slip coefficient:

$$\beta(x') = \left(\frac{6\eta}{H_c}\right)[e^{(2x'/H_c)\sqrt{5}} - 1] \tag{A13}$$

Literature Cited

Bach, P., and O. Hassager, "An Algorithm for the Use of the Lagrangian Specification in Newtonian fluid Mechanics and Application to Free Surface Flow," *J. Fluid Mech.*, **152**, 173 (1985).

Behrens, R. A., "Transient Domain Free Surface Flows and Their Applications to Mold Filling," Ph.D. Thesis, Univ. Delaware, Newark (1983).

Bhattacharji, S., and P. Savic, "Real and Apparent Non-Newtonian Behavior in Viscous Pipe Flow of Suspensions Driven by a Fluid Piston," *Proc. Heat Transfer Fluid Mech. Inst.*, 248 (1965).

Busse, W. F., "Mechanical Structures in Polymer Melts. II: Roles of Entanglements in Viscosity and Elastic Turbulence," *J. Polym. Sci.*, A2, **5**, 1261 (1967).

Castro, J. M., and C. W. Macosko, "Studies of Mold Filling and Curing in the Reaction Injection Molding Process," *AIChE J.*, **28**, 250 (1982).

Coyle, D. J., "The Kinematics of Fountain Flow in Injection Molding," 2nd Ann. Meet. Polym. Proc. Soc., Montreal (Apr., 1986).

Coyle, D. J., J. W. Blake, and C. W. Macosko, "The Kinematics of Fountain Flow in Mold-Filling," *AIChE J.*, **33**, 1168 (1987).

Dieber, J. A., and W. R. Schowalter, "Modeling the Flow of Viscoelastic Fluids Through Porous Media," *AIChE J.*, **27**, 912 (1981).

Dussan V., E. B., "The Moving Contact Line: The Slip Boundary Condition," *J. Fluid Mech.*, **77**, 665 (1976).

Elliott, G. E. P., and A. C. Riddiford, *Recent Prog. Surface Sci.*, **2**, 111 (1964).

Garner, F. H., and A. H. Nissan, "Rheological Properties of High-Viscosity Solutions of Long Molecules," *Nature*, **158**, 634 (1946).

Givler, R. C., M. J. Crochet, and R. B. Pipes, "Numerical Predictions of Fiber Orientation in Dilute Suspensions," *J. Compos. Mat.*, **17**, 330 (1983).

Gogos, C. G., C. F. Huang, and L. R. Schmidt, "The Process of Cavity Filling Including the Fountain Flow in Injection Molding," *Polym. Eng. Sci.*, **26**, 1457 (1986).

Hocking, L. M., "A Moving Fluid Interface. 2: The Removal of the Force Singularity by a Slip Flow," *J. Fluid Mech.*, **79,** 209 (1977).

Hoffman, R. L. "A Study of the Advancing Interface. I: Interface Shape in Liquid-Gas Systems," *J. Colloid Interf. Sci.*, **50,** 228 (1975).

Huang, C. F., "Simulation of the Cavity Filling Process with the Marker-and-Cell Method in Injection Molding," Ph.D. Thesis, Stevens Inst. Technol. Hoboken, NJ (1978).

Huh, C., and S. G. Mason, "The Steady Movement of a Liquid Meniscus in a Capillary Tube," *J. Fluid Mech.*, **81,** 401 (1977).

Huh, C., and L. E. Scriven, "Hydrodynamic Model of Steady Movement of a Solid/Liquid/Fluid Contact Line," *J. Colloid Interf. Sci.*, **35,** 85 (1971).

Kamal, M. R., E. Chu, P. G. Lafleur, and M. E. Ryan, "Computer Simulation of Injection Mold Filling for Viscoelastic Melts with Fountain Flow," *Polym. Eng. Sci.*, **26,** 190 (1986).

Kamal, M. R., and P. G. Lafleur, "A Structure-Oriented Computer Simulation of the Injection Molding of Viscoelastic Crystalline Polymers. II: Model Predictions and Experimental Results," *Polym. Eng. Sci.*, **26,** 106 (1986).

Lafleur, P. G., "Computer Simulation of the Injection Molding of Viscoelastic Crystalline Thermoplastics," Ph.D. Thesis, McGill Univ., Montreal (1983).

Lafleur, P. G., and M. R. Kamal, "A Structure-Oriented Computer Simulation of the Injection Molding of Viscoelastic Crystalline Polymers. I: Model with Fountain Flow, Packing, Solidification," *Polym. Eng. Sci.*, **26,** 95 (1986).

Lowndes, J., "The Numerical Simulation of the Steady Movement of a Fluid Meniscus in a Capillary Tube," *J. Fluid Mech.*, **101,** 631 (1980).

Manzione, L. T., "Simulation of Cavity Filling and Curing in Reaction Injection Molding," *Polym. Eng. Sci.*, **21,** 1234 (1981).

Mavridis, H., A. N. Hrymak, and J. Vlachopoulos, "Finite-Element Simulation of Fountain Flow in Injection Molding," *Polym. Eng. Sci.*, **26,** 449 (1986a).

———, "Finite-Element Simulation of Fountain Flow in Injection Molding," *Tech. Papers, 44th SPE ANTEC,* Boston, 103 (1986b).

———, "Deformation and Orientation of Fluid Elements Behind an Advancing Flow Front," *J. Rheol.*, **30,** 555 (1986c).

Menges, G., and G. Wübken, "Influence of Processing Conditions on Molecular Orientation in Injection Molding," *Tech. Papers, 31st SPE ANTEC,* Montreal, 519 (1973).

Metzner, A. B., Y. Cohen, and C. Rangel-Nafaile, "Inhomogeneous Flows of Non-Newtonian Fluids: Generation of Spatial Concentration Gradients," *J. Non-Newt. Fluid Mech.*, **5,** 449 (1979).

Middleman, S., *Fundamentals of Polymer Processing,* McGraw-Hill, New York (1979).

Moy, F. H., "Microstructure and the Distribution of Tensile Properties in Injection Molded Polyethylene," Ph.D. Thesis, McGill Univ., Montreal (1980).

Nakamura, K., T. Watanabe, K. Katayama, and T. Amano, "Some Aspects of Nonisothermal Crystallization of Polymers. I: Relationship Between Crystallization Temperature, Crystallinity, and Cooling Conditions," *J. Appl. Polym. Sci.*, **16,** 1077 (1972).

Orr, F. M., and L. E. Scriven, "Rimming Flow: Numerical Simulation of Steady, Viscous, Free Surface Flow with Surface Tension," *J. Fluid Mech.*, **84,** 145 (1978).

Schmidt, R. L., "A Special Mold and Tracer Technique for Studying Shear and Extensional Flows in a Mold Cavity during Injection Molding," *Polym. Eng. Sci.*, **14,** 797 (1974).

Silliman, W. J., and L. E. Scriven, "Separating Flow Near a Static Contact Line: Slip at a Wall and Shape of a Free Surface," *J. Comput. Phys.*, **34,** 287 (1980).

Tadmor, Z., "Molecular Orientation in Injection Molding," *J. App. Polym. Sci.*, **18,** 1753 (1974).

Tadmor, Z., and C. G. Gogos, *Principles of Polymer Processing,* Wiley, New York (1979).

White, J. L., and A. B. Metzner, "Development of Constitutive Equations for Polymeric Melts and Solutions," *J. Appl. Polym. Sci.*, **7,** 1867 (1963).

Winter, H. H., and K. H. Wei, "Development of Molecular Orientation in Polymer Welding Flows," *Proc. IUPAC 28th Macromol. Symp.*, 768 (1982).

Manuscript received Nov. 4, 1986, and revision received July 13, 1987.